Computers and Electronics in Agriculture 169 (2020) 105237

Contents lists available at ScienceDirect

Computers and Electronics in Agriculture

journal homepage: www.elsevier.com/locate/compag

Development and evaluation of a self-propelled electric platform for high-throughput field phenotyping in wheat breeding trials

M. Pérez-Ruiz[a,*], A. Prior[a], J. Martinez-Guanter[a], O.E. Apolo-Apolo[a], P. Andrade-Sanchez[b], G. Egea[a]

[a] Universidad de Sevilla. Área de Ingeniería Agroforestal Dpto. de Ingeniería Aeroespacial y Mecánica de Fluidos, Spain
[b] University of Arizona, Maricopa Agricultural Center Department of Biosystems Engineering, United States

ARTICLE INFO

Keywords:
Wheat breeding
Non-destructive measurements
Precision phenotyping
3D point cloud
LiDAR

ABSTRACT

The use of high-throughput phenotyping systems in crop research offers a powerful alternative to traditional methods for understanding plant behaviours. These systems provide a rapid, consistent, repeatable, non-destructive and objective sampling method to quantify complex and previously unobtainable traits at relatively fine resolutions. In this study, a field-based high-throughput phenotyping solution for wheat was developed using a sensor suite mounted on a self-propelled electric platform. A 2D LiDAR was used to scan wheat plots from overhead, while an odometry system was used as a local navigation system to determine the precise plot/plant/scan location. Accurate 3D models of the scanned wheat plots were reconstructed based on the recorded LiDAR and odometry data. Seven plots of different wheat cultivars were scanned to calculate the canopy height using LiDAR data, and these results were compared with manual ground truth measurements. Additionally, in each of these seven plots, the NDVI and PRI spectral indices were calculated using low-cost spectral reflectance sensors (SRSs) and an expensive visible/near-infrared (VIS/NIR) spectral analysis system used for reference purposes. The results of the validation showed good agreement between the LiDAR and manual wheat plant height measurements with an R^2 of 0.73 and RMSE = 2.63 cm for three days of campaign measurements. A statistically significant linear correlation was observed between the NDVI values obtained with the reference spectrometer and the low-cost SRS; the coefficients of determination were R^2 = 0.69 for day 1 and R^2 = 0.81 for day 2, suggesting a similar degree of accuracy among both sensing systems. The developed platform and the obtained wheat phenotyping results demonstrated the suitability of the system for acquiring reliable data under field conditions while maintaining a constant low speed and stability during field deployment. The adaptability of the platform to the structure of the crop and the repeatability of data collection throughout the growing season make the system suitable for integration into commercial breeding programmes.

1. Introduction

There is a general consensus regarding challenge of feeding a growing population in a world with limited resources. One approach to address this challenge is to develop new cultivars with a greater yield potential and stress tolerance; this objective can be pursued faster and more efficiently by adopting advanced technological resources. Over the last two decades, important advances in crop productivity driven by plant genetics, mechanization, automation, satellite imagery, unmanned aerial vehicle (UAV) implementation, precise pest control, and nutrient management have been achieved, and these successes have increased yields and improved food security (Griffin et al., 2017). Nevertheless, breeders still need methods that have a positive effect by increasing breeding gains, reducing the generation interval and increasing the selection intensity and accuracy, which can be supported by automated high-throughput phenotyping approaches (Rosenqvist et al., 2019). In modern plant breeding programmes, due to climate change and the dwindling suppy of irrigation water, efficient phenotyping techniques are essential for the development of new wheat varieties with high yield potential, high temperature tolerance, and improved water use efficiency or drought tolerance (Velu and Singh, 2013).

High-throughput phenotyping platforms (HTPPs) have emerged in recent years to address these needs by increasing the quality and volume of data collected during field trials of germplasm collections. Different types of HTTPs, such as the sprayer-integrated platform

* Corresponding author at: ETSIA, Ctra. Sevilla-Utrera km 1 Sevilla, 41013, Spain.
E-mail address: manuelperez@us.es (M. Pérez-Ruiz).

https://doi.org/10.1016/j.compag.2020.105237
Received 25 September 2019; Received in revised form 15 January 2020; Accepted 18 January 2020
Available online 28 January 2020

developed and evaluated at the University of Arizona (Andrade-Sanchez et al., 2014), the motorized and remote-controlled platform (Thompson et al., 2018) and the UAV-based remote sensing platform for field-based crop phenotyping (Yang et al., 2017), represent excellent examples of the application of these systems for complex data acquisition. At present, the critical need to develop proximal detection technology lies in the potential application of this technology in the field of breeding research (e.g., germplasm selection), crop response to soil or other abiotic (e.g., heat/drought stress) or biotic (e.g., disease detection) factors and the precise management of the inherent spatial and temporal variabilities of agricultural production (e.g., precision agriculture).

The majority of commercial HTPPs developed to date have been designed for use in fully-automated indoor facilities with high levels of automation, precise environmental controls and proximal sensing techniques that focus on measuring the traits of individual plants in greenhouses or growth chambers. Unfortunately, these systems are costly, and thus, they are affordable only by large transnational seed companies and the most advanced public plant research institutions globally (Araus and Cairns, 2014; Deery et al., 2014). In addition to their high cost, another major drawback is that these systems operate under controlled environments that differ greatly from the ambient conditions in the open field. Consequently, the genotypes selected for their higher performance (e.g., yield potential) under controlled environments may not retain those traits in the field (White et al., 2012).

To deploy these platforms in field environments, it is necessary to implement accurate measurement location systems, as well as onboard computer systems capable of storing and processing the acquired information. Autonomy and the ability to supply power are key to the scalability of these systems. Most recently, Bengochea-Guevara et al., 2017 described a method to perform the automatic 3D reconstruction of large areas of woody crops, such as a complete crop rows, using the Microsoft Kinect v2 sensor deployed on board of an inspection vehicle. Izard et al. (2015) developed a methodology for creating a 3D reconstruction of maize plants based on the overlapping of different georeferenced 3D point clouds provided by different orientations and time instances of light detection and ranging (LiDAR). By reducing the complexity of the platform, a significant reduction in equipment cost can be achieved. For example, the effectiveness of a local reference system based on odometry can be considered equivalent to that of an accurate location system with centimetre-scale precision, such as the real time kinematic global navigation satellite system (RTK-GNSS) receivers used in the grapevine phenotyping platform developed by Kicherer et al. (2017).

At present, the field phenotyping of complex wheat traits associated with biomass growth and grain yield is a labour-intensive process, often requiring destructive measurements that may not be representative of the entire plot and can be subject to operator error (Gérard et al., 2001). Modern phenotyping strongly relies on the use of electronic sensors, bioinformatics developments and plant modelling. Moreover, the large amount of generated information must be post- processed for further computational analysis (Zhang et al., 2010).

Laser sensors, such as LiDAR sensors, are examples of the information-intensive technologies that are used to acquire plant structure phenotypic traits. LiDAR is a widely used alternative in precision agriculture (Martínez-Guanter et al., 2017). For instance, LiDAR has many important applications in this context that range from the 3D reconstruction of crops (Xu et al., 2013; Rosell et al., 2009) to the determination of biomass (Jimenez-Berni et al., 2018) and assisted navigation of agricultural vehicles (Bechar and Vigneault, 2016).

On the basis of the above discussion, the objectives of the present study were twofold: (i) to develop an electric, low-cost and semi-automated platform with the ability to travel across a typical fields of wheat breeding trials while carrying a modular array of non-contact sensors and (ii) to test the high-throughput capacity, reproducibility and ability of the platform to measure plant heights using LiDAR technology and to capture the spectral response of wheat plants using cost-effective sensors. The crop spectral response was obtained by acquiring the normalized difference vegetation index (NDVI) and the photochemical reflectance index (PRI). The design presented in this paper was produced in full cooperation with a local breeding company to provide simple mechanical and electrical solutions for complex field phenotyping issues. The proposed system utilized readily available products for the main frame, drive train, and lightweight height-adjustable bar to hold the sensors, thereby alleviating the limitations of previous platforms.

2. Materials and methods

2.1. Experimental field

The study site was located at Escacena del Campo (Huelva, Spain), and the research was carried out during the growing season of 2018–2019. Experimental plots were sown on December 6, 2018, and the plots were harvested on June 7, 2019. These plots were managed by the breeding company Agrovegetal S.A. (latitude: 37.4525 N, longitude: 6.36194 W) as part of their breeding programme. The entire field included 75 micro-plots that were 6.25 m long and 1.20 m wide arranged in three randomized blocks containing 25 cultivars of wheat. For this study, a subset of 7 plots of different wheat cultivars were investigated: Galera, Marchena, HIR-36, Montemayor, Valbona and Gazul. The morphological variability among these cultivars was the determining factor in their selection since this variability allowed them to be characterized with the onboard instruments on board. A single irrigation event of 80 mm was uniformly applied on March 6.

2.2. Hardware setup

2.2.1. Mobile platform

The HTPP was designed to be able to travel over the plots and provide detailed, high-resolution information on the crops and individual plants at different vegetative stages (see Fig. 1). The results presented in this paper correspond to the performance of the HTPP on wheat plots. Two relevant aspects of this development are the use of non-invasive sensing technologies deployed from a height-adjustable frame to adapt to the changing vegetative stages of the crops and the implementation of an electrically powered system. As is the case for other HTPPs, this platform has three important components: a chassis-propelled electric system, a steering and directional control system, and an electronic sensing and data acquisition system.

The chassis had a main tray to carry the measurement equipment

Fig. 1. Aerial view of the assessed wheat trial plots at Escacena del Campo, Spain.

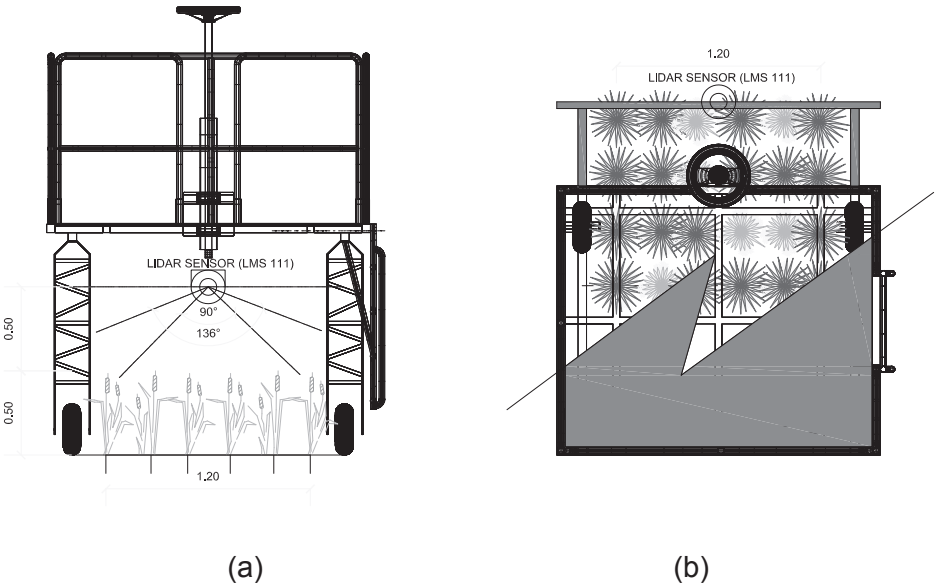

Fig. 2. Data collection platform: (A) front view and (B) top view.

and research personnel. The dimensions of this chassis were 1.9 m × 1.6 m with a ground height of 1.4 m to allow the HTTP to travel over the crops.The chassis contained the following: stairs for platform accessing the stage; handrails for personnel protection and support of auxiliary systems at heights of 0.5 and 1 m; and a platform forklift with a two-wheel drive. The chassis, handrails and forklift were structural components of the platform fabricated of tubular steel, while the stage was built with medium-density fibreboard. The structural details of the HTTP are presented in Fig. 2.

The electric drive consisted of two 24 V, 500 W DC motors with an output torque of 1.57 Nm (model EC350240, Transtecno Srl, Anzola Emilia, Italy) and was located on the forks of the wheel. The motors transmitted rotational power through their output shafts connected to the drive wheels using chains and independent sprocket wheels. These electric motors were powered by two rechargeable batteries with a capacity of 60 Ah and a working voltage of 12 V, providing full-day autonomy. The batteries were placed in the chassis tray occupying a space of 0.58 m × 0.5 m. These batteries supplied electric power supply to the computers and sensing elements of the HTPP. Overall, the self-propelled system consisted of electric motors, connected to the end wheels (rear tires) and front wheels (directional wheels).

Directional control of the vehicle was achieved through a steering wheel, which was chain-connected with sprocket wheels to a mechanism connecting rods and braces to the forks so that the steering was transmitted to all four wheels simultaneously. The steering wheel was located in the middle front of the stage to ensure that the driver was able to see both the crops and the sensor system (Fig. 3).

The design requirements, including the size limitations, drive motor torque delivery, battery size, voltage regulation, structural stability, mechanical steering, and operational safety, were evaluated and optimized. The first phase of testing was performed under controlled conditions in the laboratory with 3D-printed artificial plants, which do not present phenotypic variation.

2.2.2. Odometry system

This first HTPP prototype was used as a localization reference system and an odometry system. The shaft of an incremental optical encoder (63R256, Greyhill Inc., Illinois, USA) was mounted so that it was attached directly to the axle of the odometry wheel and used to measure the distance between two consecutive LiDAR scans (Fig. 4). This encoder generated 256 pulses per revolution, providing a 3-mm resolution in the direction of travel. The cumulative odometer pulse count was collected using a low-cost open-hardware Arduino-Leonardo microcontroller (Arduino Project, Italy) programmed in the Arduino Environment. Once collected by the microcontroller, the pulse information was sent to the computer through a USB interface, where it was fused with the LiDAR and sensor measurements.

2.2.3. Sensor systems

2.2.3.1. LiDAR. An LMS-111 LiDAR device (SICK AG, Waldkirch, Germany) was mounted on the HTTP to estimate the canopy wheat height. The sensor was set to output displacement data with a maximum scanning angle of 270°, and it was positioned facing downwards at the front of the HTTP to generate a high-density point cloud, obtaining vertical scans of objects (wheat plants and soil) with the field of view (FOV) (Fig. 5a). The basic operating principle of the LiDAR sensor is the projection of an optical signal onto the surface of an object at a certain angle and range. Processing the corresponding reflected signal time allows the sensor to determine the distance to the plant. Measurements were taken with the sensor at the centre of the plot area. Then, the actual heights of the plants were assessed to create an actual height plane (Fig. 5b). The LiDAR sensor was interfaced with a computer through an RJ45 Ethernet port for data recording. Data resolution varied with the speed of the HTTP; thus, maintaining a constant speed was of key importance for accurate measurements. The HTPP velocity was 0.27 ± 0.09 m s^{-1}, and the sensors were positioned at a height of 0.50 m over the average wheat canopy. The data acquisition software was written in the G programming language (LabVIEW™ 2015, National Instruments Co., Austin, TX, USA) and used to interface with the LiDAR sensor and odometry system. Data were written to the nonvolatile flash memory of the onboard computers.

2.2.3.2. Spectral sensors. Eight digital spectral reflectance sensors (SRS) (Meter Group, Inc. Pullman, WA, USA) with two-band radiometers were used to measure both incident and reflected radiation. The SRS were mounted on the HTPP and used for continuous monitoring of the NDVI and PRI of wheat canopies. The detectors of the PRI sensors were photodiodes paired with interference filters centred at PRI wavelengths of 532 and 570 nm PRI wavelengths, similar to those used by Garrity et al. (2010). The interference filters consist of a bandpass of 10 nm at full width at half maximum. The NDVI sensors employed photodiodes with peak sensitivities at 650 and 810 nm and a bandpass widths of 10 nm. The outputs of both sensors followed the SDI-12 standard (with

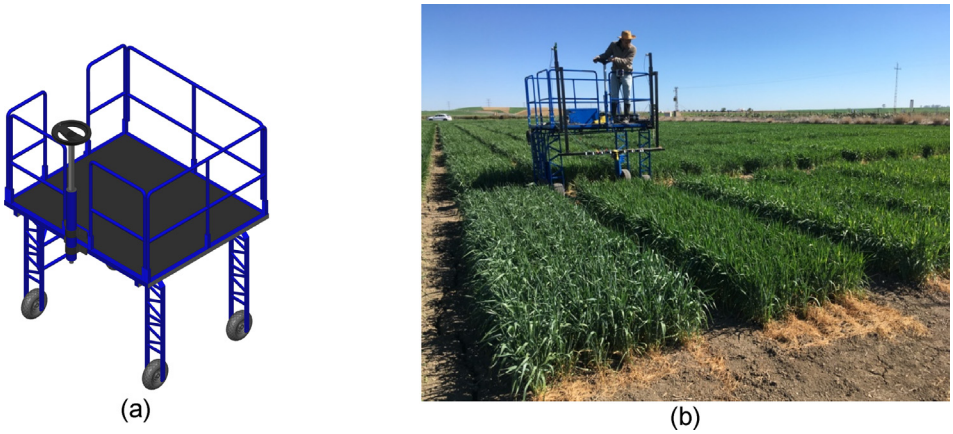

Fig. 3. (a) 3D model of the data collection platform and (b) platform in an experimental field.

Fig. 4. Ground wheel odometry system attached to the HTPP chassis.

a communication rate of 1200 bits s-1), which was anabled due to the low forward speed of the HTTP in the field and the delay between SRS measurements.

Of the four PRI sensors, three were downward-facing sensors (reflected radiation) with an FOV of approximately 36° (18° half angle), while one was an upward-facing hemispherical sensor (incident radiation) with an FOV of approximately 180° (full angle). Of the four NDVI sensors, three were downward-facing sensors (radiance measurements), and one was an upward-facing hemispherical sensors (irradiance measurement). The upward-facing hemispherical sensor (irradiance meaurements); the upward-facing hemispherical sensors provided reference values of sky irradiance, against which we normalized the downward-facing sensor values of canopy radiance using a cross-calibration method. The measurements of each sensor were logged every 18 s with an Arduino Nano datalogger V3.0, (Arduino Project, Italy), composed of a custom-made circuit board featuring solderless connectors, a real-time clock (RTC), a MicroSD memory card and a battery (7.2 V and 8000 mAh). The Arduino Nano V3.0 is an off-the-shelf part built around an ATmega328 microprocessor, which operates at 16 MHz. The datalogger includes an analogue-to-digital converter (ADC) with a 10-bit resolution (1024 voltage levels per analogue channel). To calculate reflectance, data from each of the three downward-facing PRI and NDVI (radiance) sensors were compared with the average of the coincident measurements made by the one upward-facing PRI and NDVI (irradiance) sensors, respectively. For each waveband, uncorrected reflectance was first calculated by dividing the radiance by the irradiance. These uncorrected reflectance values (Pr/Pi and Nr/Ni) calculated for each waveband were then used to calculate the uncorrected PRI (Eq. (1)) and NDVI (Eq. (2)), respectively.

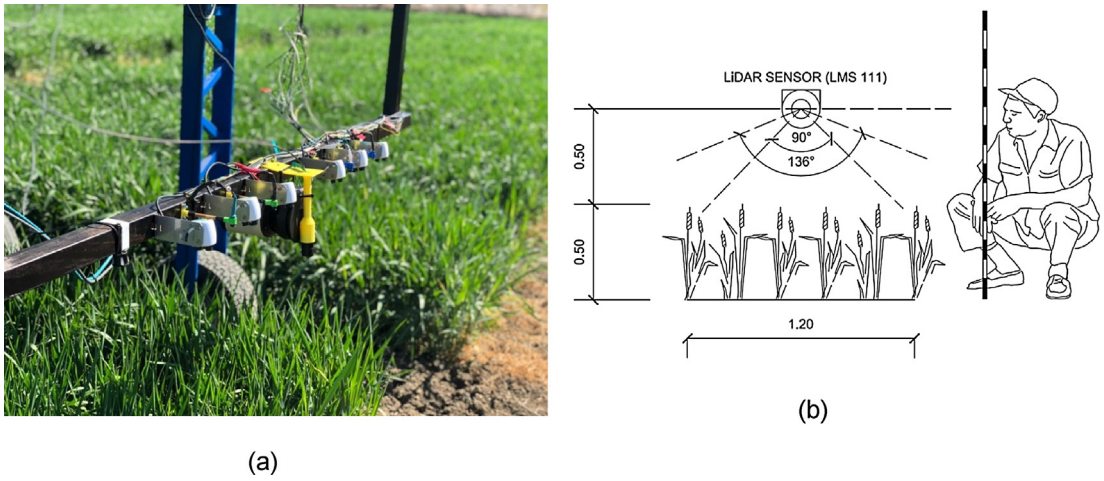

Fig. 5. (a) LiDAR, SRS and PRI sensors in field plots with the HTTP and (b) LiDAR setup for data acquisition vs manual measurements of the wheat height.

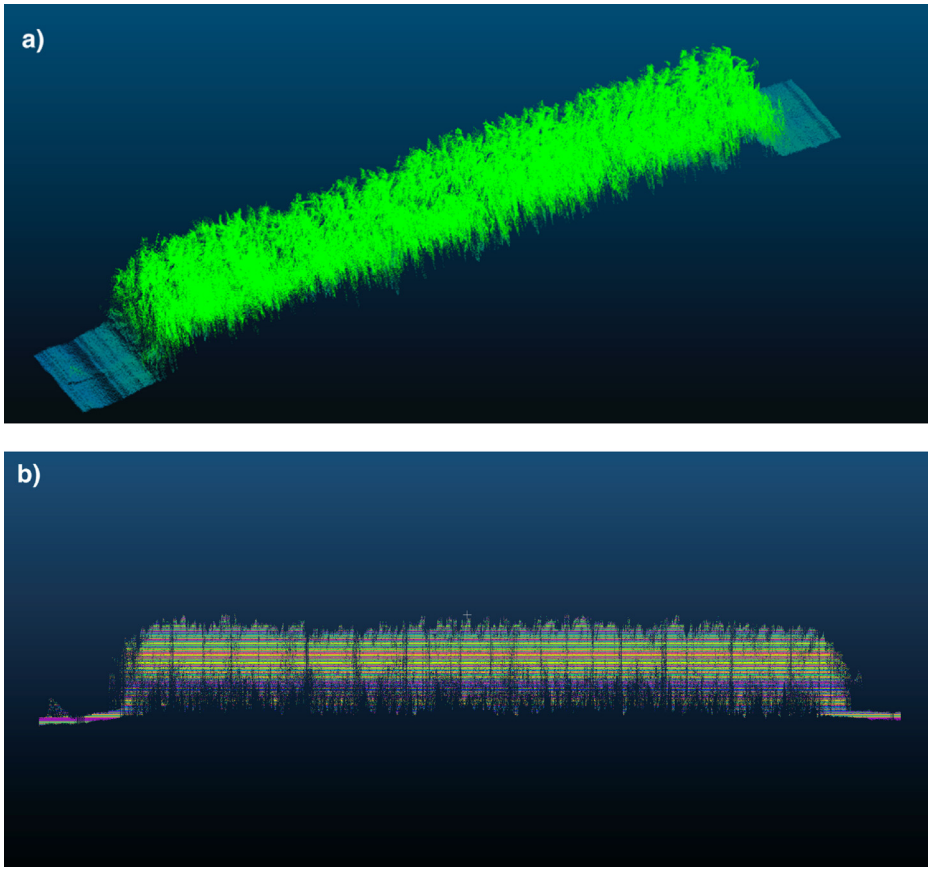

Fig. 6. (a) Selected ROI of the wheat plot, corresponding to the two central rows of wheat and (b) side view of the ROI with coloured slices of the point cloud with horizontal cutting planes.

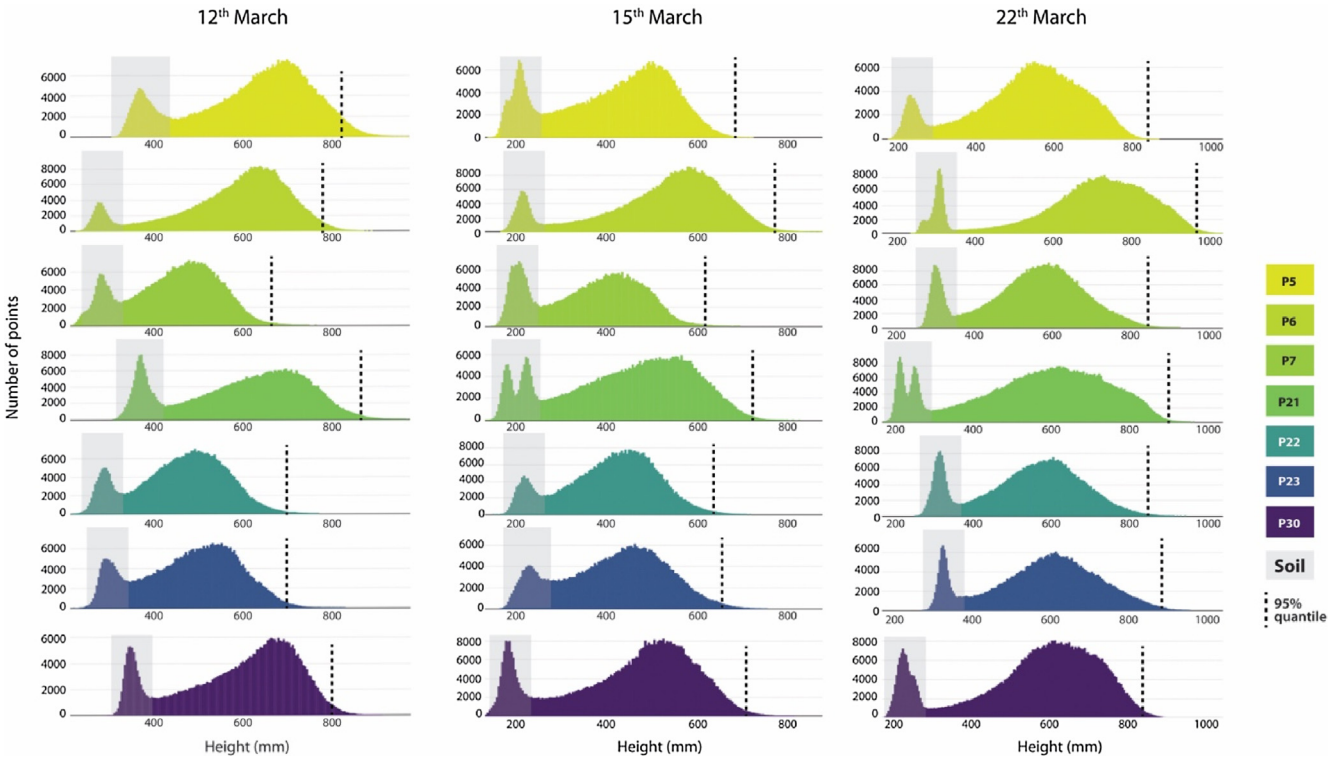

Fig. 7. Distribution of 3D points according to their heights in the point clouds obtained with LiDAR.

Table 1
Wheat canopy height values based on manual and LiDAR measurements on three dates.

	Manual		LiDAR	Manual		LiDAR	Manual		LiDAR
	Day 1 (cm)		Day 1 (cm)	Day 2 (cm)		Day 2 (cm)	Day 3 (cm)		Day 3 (cm)
Plot	Mean	Std	Value	Mean	Std	Value	Mean	Std	Value
1(5)	42.00	1.73	46.80	57.83	2.36	50.40	64.33	4.51	57.20
2(6)	49.33	3.21	50.80	56.67	1.53	56.70	68.00	2.65	64.80
3(7)	39.33	6.03	36.00	45.33	2.52	45.20	58.67	1.53	56.00
4(21)	45.66	0.58	46.80	56.83	1.04	55.60	70.33	5.03	66.00
5(22)	38.66	1.53	36.70	47.33	5.86	47.50	56.33	2.31	54.40
6(23)	42.00	1.73	43.20	50.33	4.93	50.30	57.33	3.79	56.20
7(30)	45.33	2.52	44.80	51.67	2.08	53.80	59.00	3.61	60.60
All	**43.19**	**2.48**	**43.59**	**52.29**	**2.90**	**51.36**	**62.00**	**3.35**	**59.31**

$$PRI = \frac{(PrPi)532nm - (PrPi)570nm}{(Pr/Pi)532nm + (Pr/Pi)570nm} \quad (1)$$

$$NDVI = \frac{(Pr/Pi)810nm - (Pr/Pi)650nm}{(Pr/Pi)810nm + (Pr/Pi)650nm} \quad (2)$$

Each uncorrected reflectance measurement was further modified by a sensor cross-calibration coefficient (Gamon et al., 2015), yielding the corrected reflectance and allowing us to evaluate the effect of this coefficient on the PRI or NDVI signals.

To compare and validate the measurements acquired by the low-cost SRS, a precise Unispec-DC dual-detection spectrometer (PP System, Amesbury, MA, USA) was employed as a reference. The Unispec-DC spectrometer had 256 contiguous bands for both upwelling and downwelling channels covering a nominal spectral range from approximately 310 nm to 1100 nm with an approximately 3 nm nominal bandwidth. The downward-looking detector was a fibre optic device (Uni-984, PP System, Amesbury, MA, USA) with an FOV restrictor yielding a nominal FOV of 8°. The Unispec-DC measurements were logged independently every 5 s. The spectrometer was mounted on the HTPP to obtain spectral measurements at the same time as the SRS. The upwelling channel measured incoming solar irradiance, while the downwelling channel simultaneously measured wheat canopy-reflected radiance with fibre optics, allowing measurements to be conducted under different solar radiation conditions (Hilker et al., 2010). The NDVI and PRI values computed with this research-grade spectrometer allowed the measurements recorded by the cost-effective SRS in wheat plots dedicated to plant breeding to be validated.

2.3. Measurements of wheat plant height

The height of the wheat canopy was measured using two methods: a) manual measurements with a measuring tape and b) analysis of the 3D point clouds generated with the LiDAR sensor. For the manual procedure, the height of the canopy was defined as the distance from the highest point to the lowest point above the ground. To reduce the measurement error, the measurements were repeated three times for each plot and the mean value was used.

The 3D point cloud representation of the crop obtained with the LiDAR sensor (in the form of a set of vertices in the Cartesian system), was analysed using a three-step workflow:

(i) A region of interest (ROI) was defined on the obtained point clouds of the plots to construct individual analysis elements in which the light beam of the LiDAR sensor had a zenithal incidence. This ROI corresponded in all cases to the two central rows of the wheat plots. Manual segmentation of the ROI was carried out using the manual clipping tool of CloudCompare software (CloudCompare 2.9.1 GNU License, Paris, France).

(ii) Based on the resulting point cloud, longitudinal sections (along the X-axis) with a thickness of 2 mm and a 2 mm spacing between section were generated. Each of these slice-shaped sections of the point cloud contained a variable number of points from the original cloud (Fig. 6). These sections were created automatically using the cross-section tool in the same CloudCompare software mentioned above. The information corresponding to each of the sections, namely, their elevation (Z-axis) and the number of points they contained, was exported to a file consisting of comma separated values file for further analysis.

(iii) The data extracted from the cross-sections (their heights and the number of points they contained) were analysed together. For each trial plot during the growing season, histograms and the height profiles of the point clouds were generated (Fig. 7). In this way, the cross-sectional heights corresponding to the soil and the highest part of the vegetation were determined statistically. The coordinates corresponding to the soil, which were easily distinguishable in the histograms (Fig. 7), were defined with the central value of the soil histogram. For the upper part of the vegetation, the height of the wheat was defined using the 95th percentile of the sample. In this way, the crop height caluculation ignored outliers within the calculated plant structure, such as upper wheat spikes.

The analysis was carried out in R (R Core Team, 2014), and the histograms were produced using the Plotly package (Plotly Technologies Inc., Montreal, QC, 2015).

2.4. Statistical analysis

Statistical analyses were conducted using the R software package after data sets from all the trials were collected from all the trials.

Values of Pearson's correlation coefficient, which is an index that measures the degree of covariance between linearly related variables and which ranges between −1 and +1, were obtained using ordinary least linear squares regression to assess the extents of the relationships between the wheat plant heights obtained using LiDAR and those acquired using manual methods and the relationship between the NDVI obtained with the Unispec spectrometer and the NDVI obtained with the SRS.

3. Results and discussion

3.1. Results of the wheat canopy height computations

The phenotyping platform with the LiDAR sensor was operated over seven plots during three days in March 2019, and the results of the field trials are shown in Table 1. In this study, the wheat plant height was used to assess the performance of the platform system by comparing the heights of the plants measured manually with those measured through the point cloud of the LiDAR system. The manually determined average heights were 43.10 cm for day one, 52.29 cm for day two, and 62.00 cm for day three. The results of Levene's homogeneity of variance test (Levene, 1960) showed that the standard deviation values were not significantly different (p-value < 0.05) between the days for the manual height measurements. Thus, the requirement of homogeneity requirement was met.

As depicted in Fig. 8, a good linear correlation was observed between the canopy height measured with the LiDAR sensor and the manual measurements, reflecting high similarity in the accuracy of both methods. The average coefficient of determination (R^2) was 0.73 with an average RMSE = 2.63 cm. These results are comparable to those observed by Qiu et al. 2019 in maize plants with *RMSE* = 5.80 cm. These results suggest that the LiDAR mounted on the HTTP developed in this project can be considered an alternative plant height measurement technique (Fig. 9). Compared with other methods with

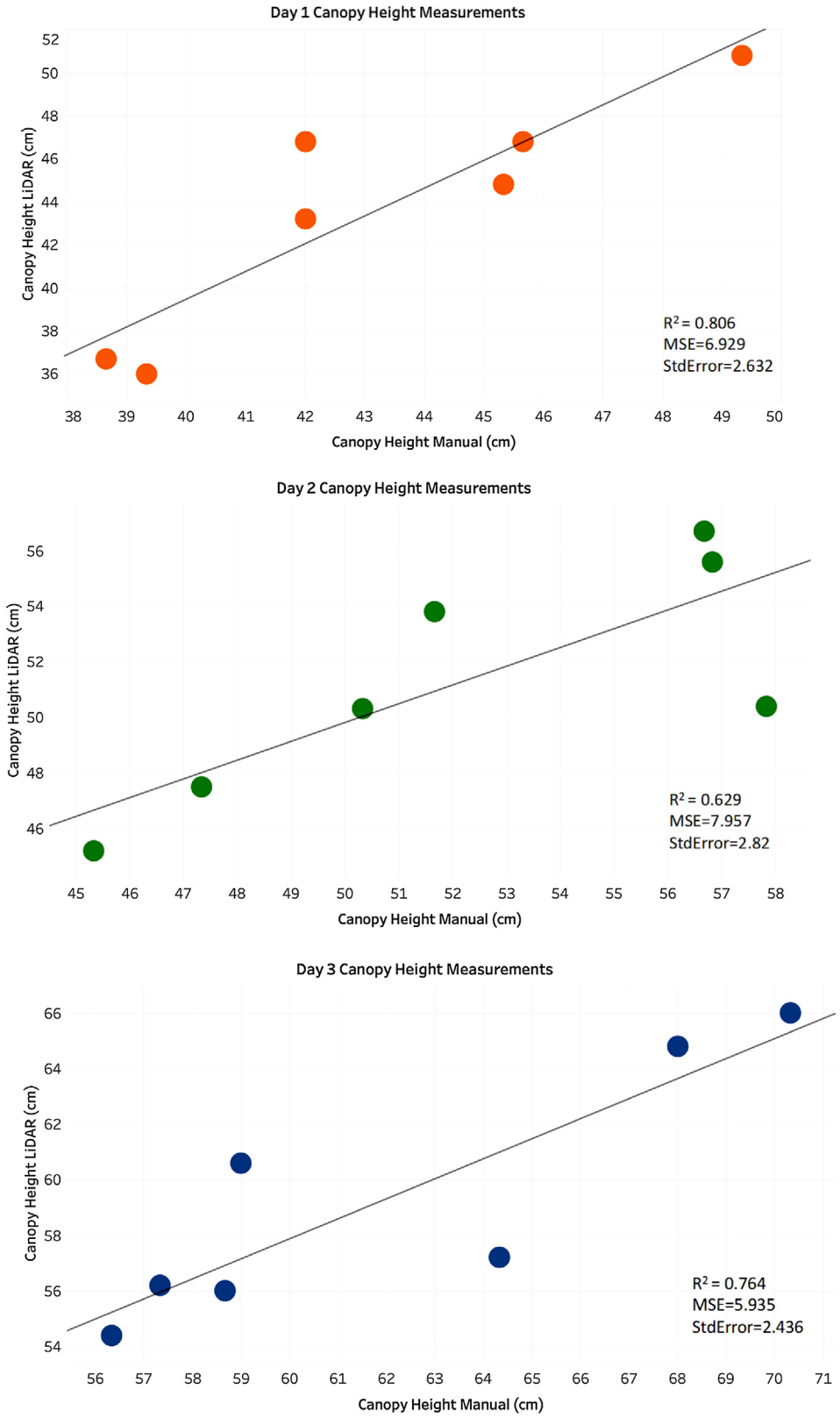

Fig. 8. Canopy height correlation between the three-day wheat measurements based on LiDAR data and the manual methodology.

RMSE = 3.50 cm (Madec et al., 2017), our method can provide an acceptable plant height accuracy in areas under proper observation conditions. Given this, we must consider that the LiDAR, despite its high resolution, did not individually characterize the plants but instead retrieved the overall canopy height. This shows its utility in biomass characterization and basic crop parameters but is weak ability to reconstruct crops in details from mobile agricultural platforms. In addition, the scanning system has been shown to be sensitive to jerky movements, which implies the need to maintain low working speeds and the need to remain on uniform terrain.

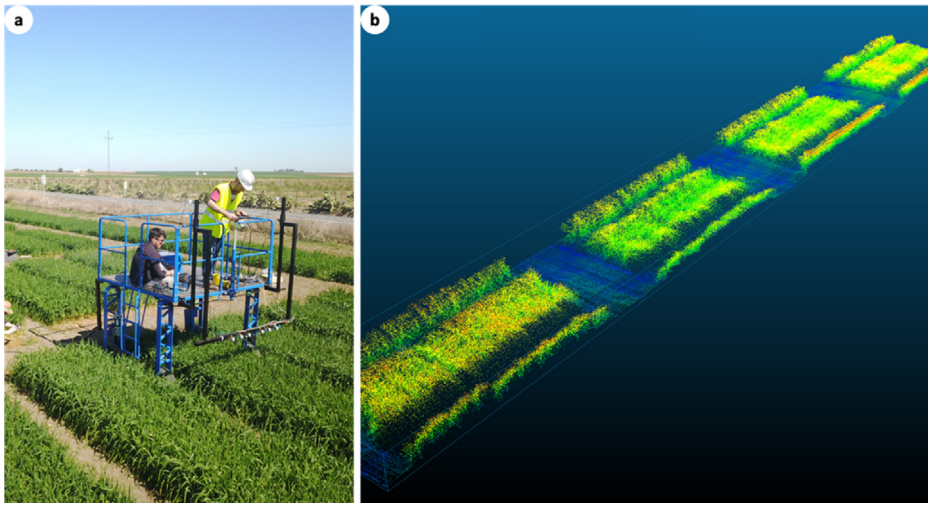

Fig. 9. (a) Wheat plots scanned during breeding trials with the developed platform and (b) LiDAR wheat point clouds generated on a set of three plots during field trials.

Table 2
Comparison between the PRI and NDVI values generated with the SRS sensors and multi-band field spectrometer.

	Unispec			
	Day 1		Day 2	
Plot	PRI	NDVI	PRI	NDVI
1(5)	−0.0533	0.880	−0.0507	0.898
2(6)	−0.0440	0.923	−0.0427	0.901
3(7)	−0.0660	0.900	−0.0512	0.916
4(21)	−0.0737	0.891	−0.1025	0.890
5(22)	−0.0594	0.913	−0.0594	0.901
6(23)	−0.1151	0.900	−0.0615	0.886
7(30)	−0.0925	0.912	−0.1019	0.901
All	**−0.0720**	**0.903**	**−0.0671**	**0.900**
	SRS			
	Day 1		Day 2	
Plot	PRI	NDVI	PRI	NDVI
1(5)	−0.0585	0.877	−0.0627	0.898
2(6)	−0.0583	0.925	−0.0501	0.898
3(7)	−0.0578	0.907	−0.0519	0.918
4(21)	−0.0630	0.869	−0.0968	0.887
5(22)	−0.0683	0.910	−0.0518	0.904
6(23)	−0.0892	0.893	−0.0550	0.890
7(30)	−0.0637	0.909	−0.0868	0.897
All	**−0.0655**	**0.899**	**−0.0650**	**0.900**

3.2. Comparing the NDVI and PRI values from the SRS and a reference field espectrometer

Table 2 shows the mean values of the NDVI and PRI indices per plot obtained with the reference spectrometer (Unispec) and the SRS. For the Unispec device, the NDVI values ranged form 0.88 to 0.92, and the PRI values varied from −0.043 to −0.115, while the NDVI values measured with the SRSs ranged from 0.87 to 0.93, and the PRI values ranged from −0.050 to −0.097.

A high linear correlation was observed (Fig. 10) between the NDVI and PRI spectral indices measured with the SRS and the high-end reference spectrometer. In a previous study, Gamon et al. (2015) observed that correcting the PRI values obtained with low-cost SRS by cross-correlation yielded values that were reasonably similar to those from a reference spectrometer. In our case study, an acceptable level of correlation was observed between the SRS and the Unispec spectrometer, although the SRS seemed to have a tendency to underestimate the PRI values. Despite this trend and the observed differences, the SRS and spectrometer yielded consistent measurements, and the results obtained can validate the use of both sensors to obtain culture parameters from this type of phenotyping platform.

4. Conclusions

The frequent deployment of instrumented platforms generates large volumes of time-series data, thereby enabling advanced data processing and analytics. HTPP-derived physiological and canopy architectural traits are highly informative and associated with the observed wheat yield variability under various degrees of water stress conditions, and these attributes provide decision-making support for unbiased selection in wheat breeding studies.

Automated and low-cost NDVI and PRI sensors offer new opportunities for monitoring photosynthetic phenology. The development and implementation of high-performance phenotyping platforms such as the one proposed in this study are of great interest to the private sector and public institutions engaged in plant breeding science with the increasing use of digital tools. Flexible, modular equipment that can adapted to the structures of the crops is key to obtaining data sets from large areas at a relatively low cost and in a timely manner. The integration and fusion of different sensors with their own communication protocols and operational characteristics for handling and capturing information constitute major challenges in these field platforms. In the future, we will continue working on a line of research dedicated to unifying and centralizing the management of all sensor information in real time, which will represent an important step and have great potential in these applications. Similarly, although the platform developed is shown to be suitable for research, its integration with an autonomous system to reduce the consumption of time and human labour during the data acquisition process will be a long-term objective.

CRediT authorship contribution statement

Manuel Pérez-Ruiz: Conceptualization, Methodology, Writing - original draft. **Alejandro Prior:** Formal Analysis. **Jorge Martínez-Guanter:** Software. **Orly Enrique Apolo-Apolo:** Investigation, Validation. **Pedro Andrade-Sanchez:** Supervision. **Gregorio Egea:** Project Administration, Funding Adquisition

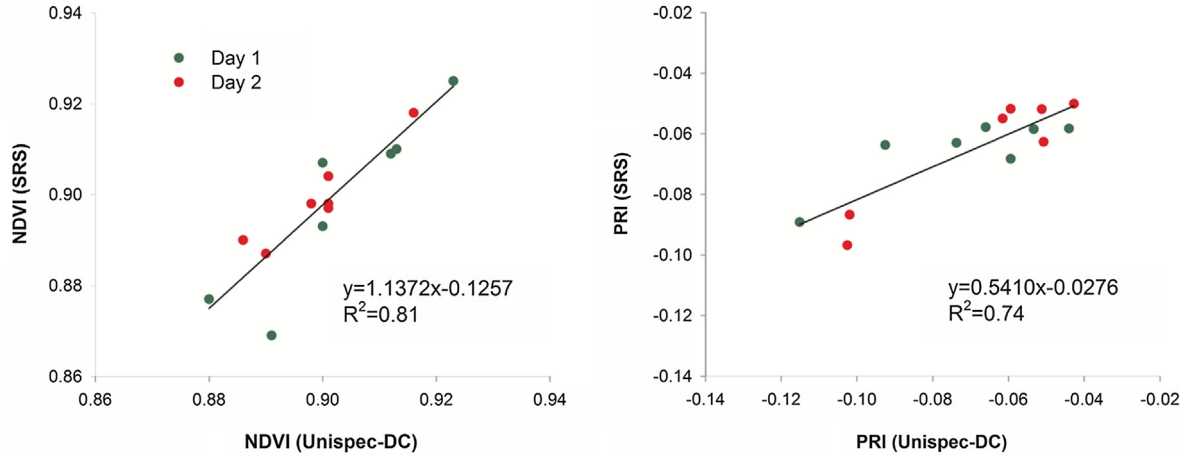

Fig. 10. Relationships between the NDVI (left) and PRI (right) plot averages obtained with a reference spectrometer multi-band instrument (Unispec-DC) and SRS.

Acknowledgements

The research was supported by the project AGL2016-78964-R funded by the Spanish Ministry of Economic and Competence. Additionally, the authors want to thank the Predoctoral Research Fellowship for the development of the University of Seville R&D&I programme (IV.3 2017) granted to OEAA and the Torres-Quevedo contract (PTQ-17-09506) granted to JMG by the Spanish Ministry of Economy.

Appendix A. Supplementary material

Supplementary data to this article can be found online at https://doi.org/10.1016/j.compag.2020.105237.

References

Andrade-Sanchez, P., Gore, M.A., Heun, J.T., Thorp, K.R., Carmo-Silva, A.E., French, A.N., Salvucci, M.E., White, J.W., 2014. Development and evaluation of a field-based high-throughput phenotyping platform. Funct. Plant Biol. 41 (1), 68–79. https://doi.org/10.1071/FP13126.

Araus, J.L., Cairns, J.E., 2014. Field high-throughput phenotyping: the new crop breeding frontier. Trends Plant Sci. 19, 52–61. https://doi.org/10.1016/j.tplants.2013.09.008.

Bechar, A., Vigneault, C., 2016. Agricultural robots for field operations: concepts and components. Bio. Eng. 149, 94–111. https://doi.org/10.1016/j.biosystemseng.2016.06.014.

Bengochea-Guevara, J.M., Andújar, D., Sanchez-Sardana, F.L., Cantuña, K., Ribeiro, A., 2018. 3D Monitoring of woody crops using a medium-sized field inspection vehicle. In: Ollero, A., Sanfeliu, A., Montano, L., Lau, N., Cardeira, C. (Eds.), ROBOT 2017: Third Iberian Robotics Conference. ROBOT 2017. Advances in Intelligent Systems and Computing. Springer, Cham.

Deery, D., Jimenez-Berni, J., Sirault, X.R.R., Jones, H.G., Furbank, R.T., Klukas, C., 2014. Proximal remote sensing buggies and potential application for phenotyping. Agronomy 4, 349–379. https://doi.org/10.3390/agronomy4030349.

Gamon, J.A., Kovalchuck, O., Wong, C.Y.S., Harris, A., Garrrity, S.R., 2015. Monitoring seasonal and diurnal changes in photosynthetic pigments with automated PRI and NDVI sensors. Biogeosciences 12, 4149–4159. https://doi.org/10.5194/bg-12-4149-2015.

Garrido Izard, Miguel; Paraforos, Dimitris S.; Reiser, David; Vázquez Arellano, Manuel; Griepentrog, Hans W. y Valero Ubierna, Constantino (2015). 3D Maize Plant Reconstruction Based on Georeferenced Overlapping LiDAR Point Clouds. "Remote Sensing", v. 7 (n. 12); p. 15870. ISSN 2072-4292.

Garrity, S.R., Vierling, L.A., Bickford, K., 2010. A simple filtered photodiode instrument for continuous measurement of narrowband NDVI and PRI over vegetated canopies. Agr. Forest Meteorol. 150, 489–496. https://doi.org/10.1016/j.agrformet.2010.01.004.

Gérard, B., Hiernaux, P., Muehlig-Versen, B., Buerkert, A., 2001. Destructive and non-destructive measurements of residual crop residue and phosphorus effects on growth and composition on herbaceous fallow species in the Sahel. Plant Soil 228, 265–273. https://doi.org/10.1023/A:1004876032203.

Griffin, T.W., Miller, N.J., Bergtold, J., Shanoyan, A., Sharda, A., Ciampitti, I.A., 2017. Farm's sequence of adoption of information-intensive precision agricultural technology. Appl. Eng. Agri. 33 (4), 521–527. https://doi.org/10.13031/aea.12228.

Hilker, T., Nesic, Z., Coops, N.C., Lessard, D., 2010. A new, automated, multiangular radiometer instrument for tower-based observations of canopy reflectance (AMSPEC II). Instrum. Sci. Technol. 38, 319–340. https://doi.org/10.1080/10739149.2010.508357.

Jimenez-Berni, J.A., Deery, D.M., Rozas-Larraondo, P., Condon, A.T.G., Rebetzke, G.J., James, R.A., Sirault, X.R., 2018. High throughput determination of plant height, ground cover, and above-ground biomass in wheat with LiDAR. Front. Plant Sci. 9, 237. https://doi.org/10.3389/fpls.2018.00237.

Kicherer, A., Herzog, K., Bendel, N., Klück, H., Backhaus, A., Wieland, M., Rose, J.C., Klingbeil, L., Läbe, T., Hohl, C., Petry, W., Kuhlmann, H., Seiffert, U., Töpfer, R., 2017. Phenoliner: A new field phenotyping platform for grapevine research. Sensors 17 (7), 1625. https://doi.org/10.3390/s17071625.

Levene, H., 1960. In Contributions to Probability and Statistics: Essays in Honor of Harold Hotelling. Stanford University Press, pp. 278–292.

Madec, S., Baret, F., de Solan, B., Thomas, S., Dutartre, D., Jezequel, S., et al., 2017. High-throughput phenotyping of plant height: comparing unmanned aerial vehicles and ground LiDAR estimates. Front. Plant Sci. 8, 2002. https://doi.org/10.3389/fpls.2017.02002.

Martínez-Guanter, J., Garrido-Izard, M., Valero, C., Slaughter, D., Pérez-Ruiz, M., 2017. Optical sensing to determine tomato plant spacing for precise agrochemical application: Two scenarios. Sensors 17 (5), 1096. https://doi.org/10.3390/s17051096.

Qiu, Q., Sun, N., Bai, H., Wang, N., Fan, Z., Wang, Y., Meng, Z., Li, B., Cong, Y., 2019. Field-based high-throughput phenotyping for maize plant using 3D LiDAR point cloud generated with a "phenomobile". Front. Plant Sci. 10, 554. https://doi.org/10.3389/fpls.2019.00554.

Rosell, J.R., Llorens, J., Sanz, R., Arno, J., Ribes-Dasi, M., et al., 2009. Obtaining the three-dimensional structure of tree orchards from remote 2D terrestrial LIDAR scanning. Agri. Forest Meteorol. 149 (9), 1505–1515. https://doi.org/10.1016/j.agrformet.2009.04.008.

Rosenqvist, E., GroBkinsky, D.K., Ottosen, C., van de Zedde, R., 2019. The phenotyping dilemma-The challenges of the diversified phenotyping community. Front. Plant Sci. 10, 163. https://doi.org/10.3389/fpls.2019.00163.

Thompson, A.L., Conrad, A., Conley, M.M., Shrock, H., Taft, B., Miksch, C., Mills, T., Dyer, J.M., 2018. Professor: A motorized field-based phenotyping cart. HardwareX 4, e00025. https://doi.org/10.1016/j.ohx.2018.e00025.

Velu, G. and Singh, R.P., 2013. Phenotyping in Wheat Breeding. Phenotyping for Plant Breeding: Applications of Phenotyping Methods for Crop Improvement. S.K. Panguluri and A.A. Kumar (eds.). https://doi.org/0.1007/978-1-4614-8320-5.

White, J.W., Andrade Sanchez, P., Gore, M.A., Bronson, K.F., Coffelt, T.A., Conley, M.M., Feldmann, K.A., French, A.N., Heun, J.T., Hunsaker, D.J., Jenks, M.A., Kimball, B.A., Roth, R.L., Strand, R.J., Thorp, K.R., Wall, G.W., Wang, G., 2012. Field-based phenomics for plant genetics research. Field Crops Res 133, 101–112. https://doi.org/10.1016/j.fcr.2012.04.003.

Xu, W., Su, Z., Feng, Z., Xu, H., Jiao, Y., Yan, F., 2013. Comparison of conventional measurement and LiDAR-based measurement for crown structures. Comput. Electronics Agri. 98, 242–251. https://doi.org/10.1016/j.compag.2013.08.015.

Zhang, W., Li, F., Nie, L., 2010. Integrating multiple 'omics' analysis for microbial biology: application and methodologies. Microbiology 156 (2), 287–301. https://doi.org/10.1099/mic.0.034793-0.